Multi-Atlas Propagation Based Left Atrium Segmentation Coupled with Super-Voxel Based Pulmonary Veins Delineation in Late Gadolinium-Enhanced Cardiac MRI

Guang Yang [†a,b], Xiahai Zhuang [†c], Habib Khan [a,b], Shouvik Haldar [a], Eva Nyktari [a], Lei Li [c], Xujiong Ye [d], Greg Slabaugh [e], Tom Wong [a], Raad Mohiaddin [a,b], Jennifer Keegan [‡a,b], and David Firmin [‡a,b]

[a] Cardiovascular Biomedical Research Unit, Royal Brompton Hospital, SW3 6NP, London, UK;
[b] National Heart & Lung Institute, Imperial College London, SW7 2AZ, London, UK;
[c] SJTU-CU International Cooperative Research Centre, Department of Engineering Mechanics, Shanghai Jiao Tong University, Shanghai, 200240, China;
[d] School of Computer Science, University of Lincoln, LN6 7TS, Lincoln, UK;
[e] Department of Computer Science, City University London, EC1V 0HB, London, UK.

ABSTRACT

Late Gadolinium-Enhanced Cardiac MRI (LGE CMRI) is a non-invasive technique, which has shown promise in detecting native and post-ablation atrial scarring. To visualize the scarring, a precise segmentation of the left atrium (LA) and pulmonary veins (PVs) anatomy is performed as a first step—usually from an ECG gated CMRI roadmap acquisition—and the enhanced scar regions from the LGE CMRI images are superimposed. The anatomy of the LA and PVs in particular is highly variable and manual segmentation is labor intensive and highly subjective. In this paper, we developed a multi-atlas propagation based whole heart segmentation (WHS) to delineate the LA and PVs from ECG gated CMRI roadmap scans. While this captures the anatomy of the atrium well, the PVs anatomy is less easily visualized. The process is therefore augmented by semi-automated manual strokes for PVs identification in the registered LGE CMRI data. This allows us to extract more accurate anatomy than the fully automated WHS. Both qualitative visualization and quantitative assessment with respect to manual segmented ground truth showed that our method is efficient and effective with an overall mean Dice score of 0.91.

Keywords: Atlas Propagation, Multi-Scale Patch, Local Atlas Ranking, Whole Heart Segmentation, Super-Voxel, Cardiac MRI, Medical Imaging Analysis, Image Processing

1. INTRODUCTION

Late Gadolinium-Enhanced Cardiac MRI (LGE CMRI) is an emerging non-invasive technique to identify native and post-ablation atrial scarring and shows potential to replace the current invasive clinical gold standard of electro-anatomical mapping (EAM) [1]. While studies have shown inverse correlation between image intensity in the LGE CMRI and left atrium (LA) endocardial voltage obtained from the EAM, there is on-going concerns regarding the reproducibility of the LGE CMRI technique [2]. This can partly be attributed to the fact that atrial scarring identification generally relies on manually segmented anatomy of the LA and pulmonary veins (PVs), which is not only time-consuming but also highly subjective among human operators and different research institutions [3]. The anatomy may be

segmented from a respiratory and ECG gated CMRI roadmap acquisition or from rapidly acquired breath-hold MR angiography (MRA) [4,5]. While the latter is faster, the lack of ECG gating leads to mis-registration with the respiratory and ECG gated LGE CMRI dataset and the former is preferred. The purpose of this work is to design an objective, efficient and accurate segmentation method for the delineation of the LA and PVs that can be applied to the LGE CMRI images with minimum human intervention. Results on 20 LGE CMRI scans of atrial fibrillation patients show the promise of our method for further deployment in clinical environment.

2. METHODOLOGY

The overall framework of our method is summarized as shown in the flowchart in Figure 1.

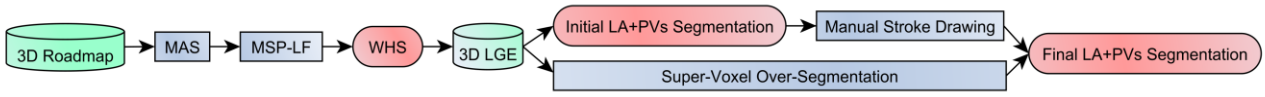

Figure 1: Flowchart of our approach including both whole heart segmentation (WHS) and super-voxel (SV) based refinements.

2.1 Multi-Atlas Propagation Based Fully-Automated Whole Heart Segmentation (WHS)

First, a multi-atlas propagation based segmentation (MAS) [6] was developed and applied to the steady-state free precession (b-SSFP) CMRI whole-heart (a.k.a. CMRI roadmap) acquisition and followed by a multi-scale patch based label fusion (MSP-LF) [7] (Figure 1). This derived labels of four chambers, major vessels and PVs. We extracted the LA and PVs as the initial segmentation. As both roadmap and LGE CMRI sequences are ECG gated and respiratory navigated, we can apply the extracted LA and PVs segmentation from the roadmap directly to the LGE CMRI images.

2.2 Semi-Automated Super-Voxel Refinement

Second, we look through the initial segmentation overlaid on the 3D LGE CMRI images to see if any PVs have been poorly identified or missed. If so, manual strokes are drawn in the LGE CMRI image to identify the missing PVs.

Meanwhile, a 3D super-voxel (SV) technique is applied for each LGE CMRI volume [8]. We applied a SLIC (Simple Linear Iterative Clustering) based SV method, which has been proved to be effective and efficient in many medical image analysis problems [9–11]. SV is an unsupervised learning [12] based method that over-segments the images into meaningful sub-regions. In addition, we applied a SV technique that adaptively chooses the compactness parameter, which controls the shape of SVs. This method is particularly designed for medical images, and the only parameter that needs to be tuned is the number of the SVs [13].

Lastly, the SVs overlapped with manual strokes are included in the final segmentation. Because the SVs are calculated in 3D space, only a small number of 2D manual strokes are required to capture the missed PVs in 3D.

3. EXPERIMENTS AND RESULTS

Figure 2 shows a single slice from an example 3D LGE MRI study (a), the initial WHS based segmentation (green boundary) with manually drawn strokes (in red) (b), and the 3D SV grid (c). Comparisons of the manually drawn ground truth (purple boundary) (d), initial automatic segmentation (green boundary) (e), and final segmentation (cyan boundary) (f) are also shown.

Table **1** tabulates the Dice score (0.91±0.08) and the Jaccard index (0.84±0.10) [14] of the final segmentation calculated with respect to the ground truth. Figure 3 (a) shows that our final segmentation has significant improvements compared to the initial segmentation based on the WHS alone. In order to determine the optimal number of SVs, we considered both the consistency of the SV derived boundary with the manually drawn ground truth, and the running time of the 3D SV calculation. The former was computed as a training procedure before the input of manual strokes on one randomly selected patient data. Figure 3 (b) shows the analysis with different numbers of SVs. Finally, we used $n = 160\text{k}$ SVs per 3D LGE volume (running time $t \approx 45$ seconds per volume). Figure 4 shows the segmentation results (3D rendering) of three example cases.

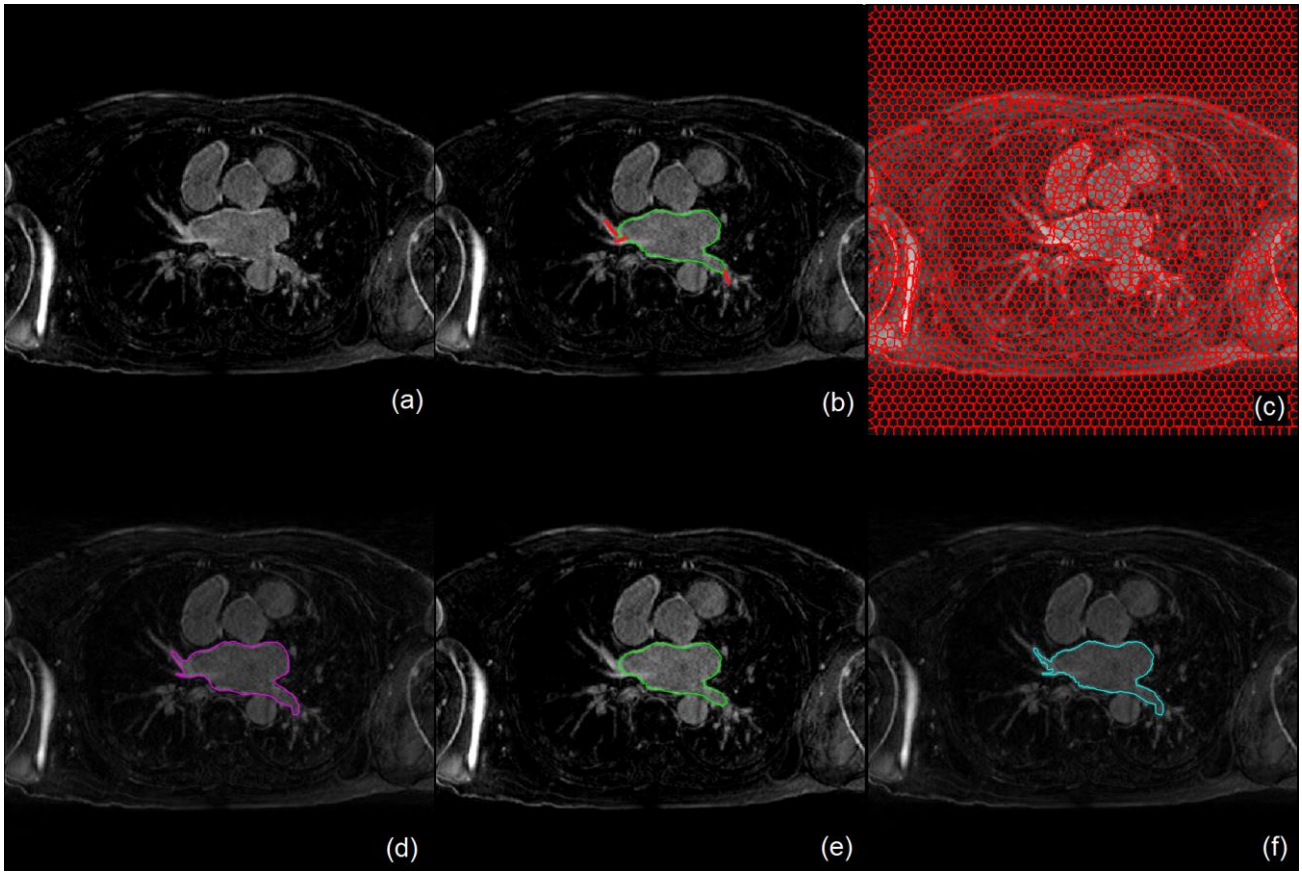

Figure 2: (a) A single slice of a 3D LGE CMRI image where scarred tissue is seen as high signal intensity; (b) Green boundary: initial segmentation of the LA and PVs using WHS showing missed (right superior) and truncated (left inferior) PVs; Red strokes: manually drawn searching directions of the missed or underestimated PVs; (c) SV based over-segmentation (grid in red) overlaid on the LGE CMRI slice; (d) Purple boundary: manual drawn ground truth of the LA and PVs; (e) Green boundary: initial segmentation of the LA and PVs using WHS; (f) Cyan boundary: final LA and PVs segmentation.

4. DISUSSION AND CONCLUSION

In this study, we proposed a semi-automated segmentation method for accurate delineation of LA and PVs, which is based on multi-atlas propagation and SV refinement. The SV refinement provides us an opportunity to modify and improve the segmentation results obtained from the fully-automated WHS method. This is particularly useful when we have variable anatomical structures, for example, LA and PVs. Although the SV refinement involves further manual intervention, the method has been proved to be efficient. In summary, both qualitative visual appearances and quantitative results have demonstrated that our method can achieve promising segmentation results with minimum human intervention.

Table 1: Quantitative evaluation of the final LA and PVs segmentation after semi-automated SV refinement.

Evaluation Methods	**Patient Number (Number of Slices Covering the LA)**							
	1 (33)	2 (35)	3 (41)	4 (35)	5 (37)	6 (36)	7 (34)	8 (36)
Dice Score	0.919±0.063	0.921±0.062	0.924±0.065	0.896±0.066	0.887±0.064	0.907±0.055	0.913±0.065	0.919±0.052
Jaccard Index	0.856±0.099	0.859±0.096	0.865±0.098	0.818±0.102	0.803±0.088	0.835±0.089	0.846±0.101	0.854±0.086

Evaluation Methods	**Patient Number (Number of Slices Covering the LA)**							
	9 (37)	10 (35)	11 (32)	12 (35)	13 (35)	14 (26)	15 (32)	16 (35)
Dice Score	0.919±0.032	0.876±0.109	0.897±0.050	0.906±0.038	0.919±0.047	0.903±0.098	0.881±0.091	0.917±0.062
Jaccard Index	0.852±0.053	0.794±0.153	0.817±0.077	0.831±0.062	0.854±0.077	0.835±0.141	0.798±0.125	0.852±0.098

Evaluation Methods	**Patient Number (Number of Slices Covering the LA)**				
	17 (47)	18 (36)	19 (38)	20 (36)	**Overall (-)**
Dice Score	0.900±0.055	0.910±0.157	0.907±0.057	0.919±0.066	**0.907±0.075**
Jaccard Index	0.823±0.085	0.856±0.161	0.834±0.088	0.856±0.093	**0.837±0.104**

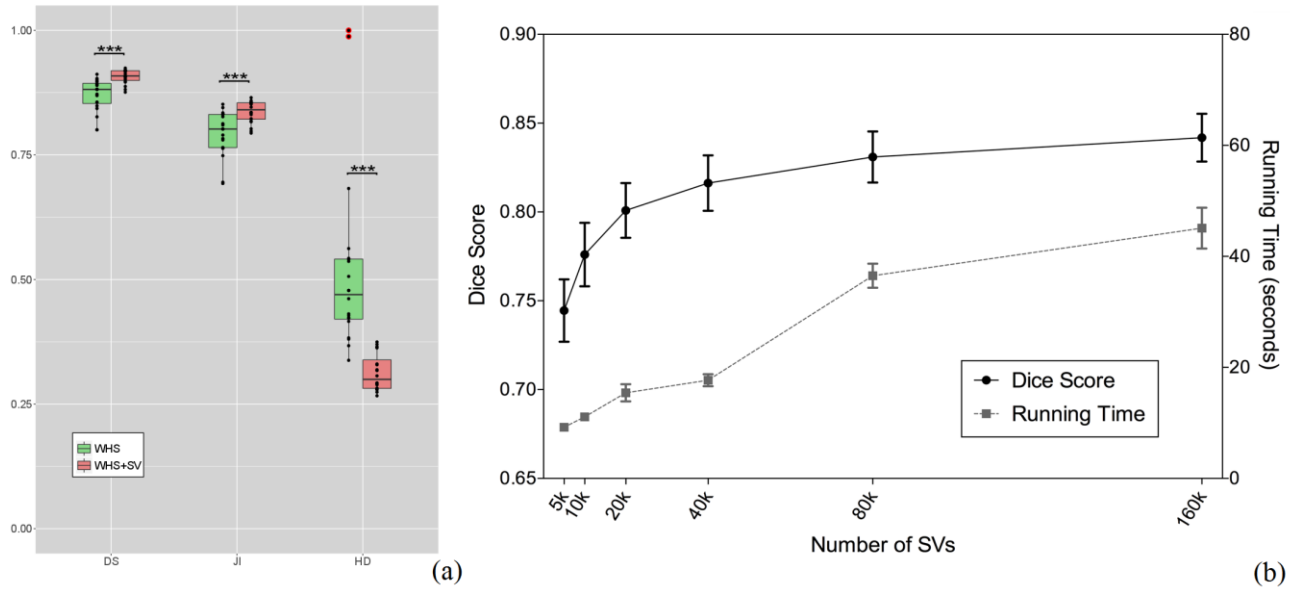

Figure 3: (a) Boxplot of comparing the initial and final LA and PVs segmentation using evaluation metrics, i.e., Dice score (DS), Jaccard index (JI) and the normalized Hausdorff distance (HD); Statistical significances (indicated by '***') were given by two-sample Wilcoxon rank-sum test between the initial and final segmentation results with significance level of $p<0.05$ (DS: p = 1.14e-05, JI: p = 1.55e-04 and HD: p = 6.53e-10); (b) Dice scores and running times with respect to different number of SVs.

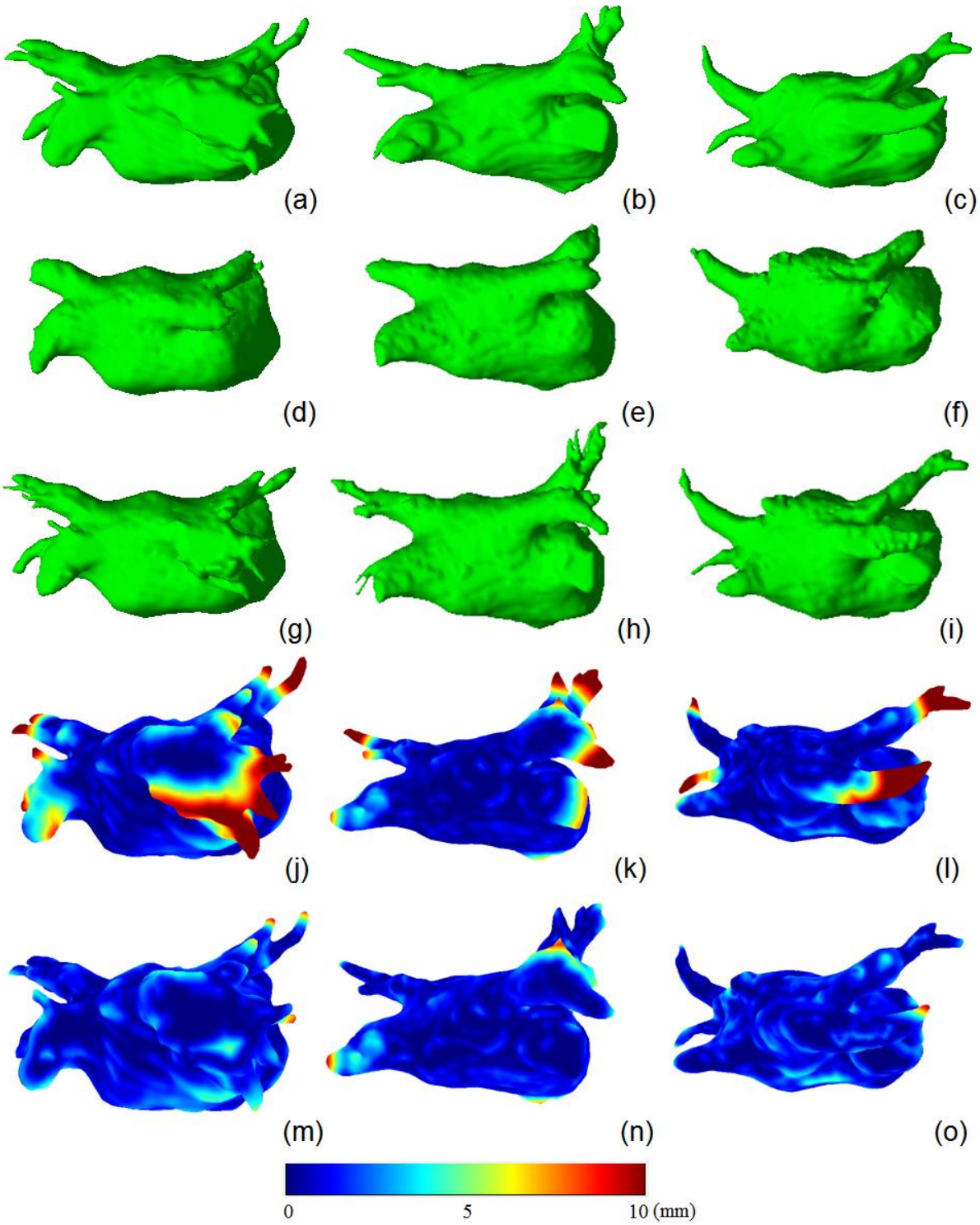

Figure 4: Segmentation results (3D rendering) of three example cases are illustrated in three columns. (a)-(c) Manual delineated ground truth; (d)-(f) Initial LA and PVs segmentation based on fully-automated WHS; (g-i) Final LA and PVs segmentation after semi-automated SV refinement; (j-l) Hausdorff distance (in mm) between the ground truth and initial LA and PVs segmentation based on WHS; (m-o) Hausdorff distance (in mm) between the ground truth and final LA and PVs segmentation after semi-automated SV refinement.

REFERENCES

[1] Calkins, H., Kuck, K. H., Cappato, R., Brugada, J., Camm, A. J., Chen, S.-A., Crijns, H. J. G., Damiano, R. J., Davies, D. W., et al., "2012 HRS/EHRA/ECAS expert consensus statement on catheter and surgical ablation of atrial fibrillation: recommendations for patient selection, procedural techniques, patient management and follow-up, definitions, endpoints, and research trial design," Heart Rhythm 9(4), 632–696.e21 (2012).

[2] Harrison, J. L., Sohns, C., Linton, N. W., Karim, R., Williams, S. E., Rhode, K. S., Gill, J., Cooklin, M., Rinaldi, C. a., et al., "Repeat Left Atrial Catheter Ablation: Cardiac Magnetic Resonance Prediction of Endocardial Voltage and Gaps in Ablation Lesion Sets," Circ. Arrhythmia Electrophysiol. 8(2), 270–278 (2015).

[3] Karim, R., Housden, R. J., Balasubramaniam, M., Chen, Z., Perry, D., Uddin, A., Al-Beyatti, Y., Palkhi, E., Acheampong, P., et al., "Evaluation of current algorithms for segmentation of scar tissue from late gadolinium enhancement cardiovascular magnetic resonance of the left atrium: an open-access grand challenge.," J. Cardiovasc. Magn. Reson. 15, 105–122 (2013).

[4] Knowles, B. R., Caulfield, D., Cooklin, M., Rinaldi, C. A., Gill, J., Bostock, J., Razavi, R., Schaeffter, T.., Rhode, K. S., "3-D visualization of acute RF ablation lesions using MRI for the simultaneous determination of the patterns of necrosis and edema," IEEE Trans. Biomed. Eng. 57(6), 1467–1475 (2010).

[5] Tao, Q., Ipek, E. G., Shahzad, R., Berendsen, F. F., Nazarian, S.., van der Geest, R. J., "Fully automatic segmentation of left atrium and pulmonary veins in late gadolinium-enhanced MRI: Towards objective atrial scar assessment.," J. Magn. Reson. Imaging 44(2), 346–354 (2016).

[6] Zhuang, X., Rhode, K. S., Razavi, R. S., Hawkes, D. J.., Ourselin, S., "A registration-based propagation framework for automatic whole heart segmentation of cardiac MRI," IEEE Trans. Med. Imaging 29(9), 1612–1625 (2010).

[7] Zhuang, X.., Shen, J., "Multi-scale patch and multi-modality atlases for whole heart segmentation of MRI," Med. Image Anal. 31, 77–87, Elsevier B.V. (2016).

[8] Achanta, R., Shaji, A., Smith, K.., Lucchi, A., "SLIC superpixels compared to state-of-the-art superpixel methods," IEEE Trans. Pattern Anal. Mach. Intell. 34(11), 2274–2281 (2012).

[9] Soltaninejad, M., Yang, G., Lambrou, T., Allinson, N., Jones, T. L., Barrick, T. R., Howe, F. A.., Ye, X., "Automated brain tumour detection and segmentation using superpixel-based extremely randomized trees in FLAIR MRI.," Int. J. Comput. Assist. Radiol. Surg. (2016).

[10] Soltaninejad, M., Ye, X., Yang, G., Allinson, N.., Lambrou, T., "An image analysis approach to MRI brain tumour grading," Oncol. News 9(6), 204–207 (2015).

[11] Soltaninejad, M., Ye, X., Yang, G., Allinson, N.., Lambrou, T., "Brain tumour grading in different MRI protocols using SVM on statistical features," Med. Image Underst. Anal., British Machine Vision Association (2014).

[12] Yang, G., Raschke, F., Barrick, T. R.., Howe, F. A., "Manifold Learning in MR Spectroscopy using Nonlinear Dimensionality Reduction and Unsupervised Clustering," Magn. Reson. Med. 74(3), 868–878 (2015).

[13] Holzer, M.., Donner, R., "Over-Segmentation of 3D Medical Image Volumes based on Monogenic Cues," 19th Comput. Vis. Winter Work., 35–42 (2014).

[14] Yang, G., Hipwell, J. H., Clarkson, M. J., Tanner, C., Mertzanidou, T., Gunn, S., Ourselin, S., Hawkes, D. J.., Arridge, S. R., "Combined reconstruction and registration of digital breast tomosynthesis," Lect. Notes Comput. Sci. (including Subser. Lect. Notes Artif. Intell. Lect. Notes Bioinformatics) 6136 LNCS, 760–768 (2010).

† indicates corresponding authors G.Y. (g.yang@imperial.ac.uk) and X.H.Z. (zhuangxiahai@sjtu.edu.cn).
‡ indicates joint senior authors.

This study was funded by the British Heart Foundation Project Grant (Project Number: PG/16/78/32402) and the NIHR Cardiovascular Biomedical Research Unit, Royal Brompton Hospital & Harefield NHS Foundation Trust and Imperial College London. Data were obtained during the NIHR Efficacy and Mechanism Evaluation Programme (Project Number: 12/127/127).